



The Interacting Late-type Host Galaxy of the Radio-loud Narrow-line Seyfert 1 IRAS 20181-2244

M. Berton^{1,2} , E. Congiu^{3,4} , S. Ciroi^{3,5} , S. Komossa⁶ , M. Frezzato³, F. Di Mille⁷ , S. Antón⁸ , R. Antonucci⁹, A. Caccianiga⁴ , P. Coppi¹⁰, E. Järvelä^{2,11}, J. Kotilainen¹ , A. Lähteenmäki^{2,11}, S. Mathur¹², S. Chen^{3,13,14}, V. Cracco³, G. La Mura¹⁵ , and P. Rafanelli³

¹ Finnish Centre for Astronomy with ESO (FINCA), University of Turku, Quantum, Vesilinnantie 5, FI-20014 University of Turku, Finland; marco.berton@utu.fi

² Aalto University Metsähovi Radio Observatory, Metsähovintie 114, FI-02540 Kylmäla, Finland

³ Dipartimento di Fisica e Astronomia “G. Galilei,” Università di Padova, Vicolo dell’Osservatorio 3, I-35122 Padova, Italy

⁴ INAF—Osservatorio Astronomico di Brera, via E. Bianchi 46, I-23807 Merate (LC), Italy

⁵ INAF—Osservatorio Astronomico di Padova, Vicolo dell’Osservatorio 5, I-35122 Padova, Italy

⁶ Max-Planck-Institut für Radioastronomie, Auf dem Hügel 69, D-53121 Bonn, Germany

⁷ Las Campanas Observatory, Carnegie Institution of Washington, Colina El Pino Casilla 601, La Serena, Chile

⁸ CIDMA, Department of Physics, University of Aveiro, 3810-193, Aveiro, Portugal

⁹ Department of Physics, University of California, Santa Barbara, CA 93106-9530, USA

¹⁰ Yale Center for Astronomy and Astrophysics, Yale University, New Haven, CT 06520-8121, USA

¹¹ Aalto University Department of Electronics and Nanoengineering, P.O. Box 15500, FI-00076 AALTO, Finland

¹² Department of Astronomy and Center for Cosmology and AstroParticle Physics, The Ohio State University, 140 West 18th Avenue, Columbus, OH 43210, USA

¹³ Center for Astrophysics, Guangzhou University, 510006, Guangzhou, People’s Republic of China

¹⁴ Istituto Nazionale di Fisica Nucleare (INFN), Sezione di Padova, I-35131, Padova, Italy

¹⁵ Laboratory of Instrumentation and Experimental Particle Physics, Av. Prof. Gama Pinto, 2-1649-003 Lisboa, Portugal

Received 2018 July 21; revised 2018 November 18; accepted 2018 December 2; published 2019 January 14

Abstract

Narrow-line Seyfert 1 galaxies (NLS1s) are a class of active galactic nuclei that are known to be one of the few sources of γ -rays, which originate in a relativistic beamed jet. Because of their relatively large distance, a poorly investigated aspect of these jetted NLS1s is their environment, and in particular, their host galaxy. In this work, we present the results of a morphological analysis of the host galaxy of the jetted NLS1 IRAS 20181-2244 observed with the 6.5 m Baade Telescope of the Las Campanas Observatory. The GALFIT analysis run on the K_s image, along with additional spectroscopic observations performed with the Nordic Optical Telescope, clearly revealed the presence of an interacting system of two galaxies. The data suggest that this NLS1 is hosted by a late-type galaxy, although the result is not conclusive. This analysis, along with other results in the literature, might suggest that two populations of jetted NLS1 exist. Further morphological studies are needed to confirm or disprove this hypothesis.

Key words: galaxies: active – galaxies: peculiar – galaxies: photometry – galaxies: Seyfert

1. Introduction

For many years it was believed that radio-loud¹⁶ active galactic nuclei (AGNs), and quasars in particular, were hosted in giant elliptical galaxies (Laor 2000; Chiaberge & Marconi 2011). Powerful relativistic jets were indeed observed in systems hosting very massive black holes that, as shown by the $M_{\text{BH}}-\sigma_*$ relation (Ferrarese & Merritt 2000), are found in ellipticals. The jet power, however, directly scales with the black hole mass (Heinz & Sunyaev 2003; Foschini 2011). Relativistic jets launched by high-mass black holes are more powerful and easier to detect. More recent studies, in fact, detected relativistic jets in spiral galaxies (e.g., Mao et al. 2015). Furthermore, the high sensitivity of the *Fermi*/Large Area Telescope (LAT) Satellite led to the discovery of γ -ray emission coming from narrow-line Seyfert 1 galaxies (NLS1; Abdo et al. 2009a, 2009b), indicating the presence of relativistic jets in a fraction of these AGN.

Classified according to their spectral properties (Osterbrock & Pogge 1987; Goodrich 1989), NLS1s show narrow permitted lines which, unlike in type 2 AGN, are not attributed to obscuration. The presence of strong Fe II multiplets in the

spectrum, in fact, indicates that the broad-line region (BLR) is directly visible. NLS1s are often considered young (i.e., galactic nuclei in their first activity phase; Mathur 2000; Mathur et al. 2001; Kawakatu et al. 2007; Wang & Zhang 2007; Foschini et al. 2015; Berton et al. 2017, 2018) or rejuvenated AGN (Mathur et al. 2012). These objects harbor a relatively low-mass black hole ($10^6-10^8 M_{\odot}$) estimated via a single epoch virial technique; Peterson 2011) accreting close to the Eddington limit (Boroson & Green 1992) growing fast and evolving toward high-mass objects (Mathur et al. 2001). This relatively low gravitational potential induces a low rotational velocity in the gas, which translates into the narrow lines. However, a disk-like geometry of the BLR might also account for the narrow lines if observed pole-on because of the lack of Doppler broadening. If in some sources inclination plays a major role, the virial technique may underestimate their black hole mass. These low-inclination NLS1s then may not harbor a low-mass black hole and, possibly, be different with respect to other NLS1s (Sulentic et al. 2000; Decarli et al. 2008; Shen & Ho 2014).

A way to distinguish between low-mass and low-inclination NLS1s is by means of host galaxy studies. The host galaxy can be an independent indicator of the black hole mass. While late-type hosts can be associated with lower masses, in fact, ellipticals typically harbor high-mass black holes (e.g., Salucci et al. 2000; Kormendy & Ho 2013, and references therein). For

¹⁶ Radio loudness is defined as the ratio, R , between the 5 GHz and the optical B -band flux densities (Kellermann et al. 1989). A source is considered radio loud if $R > 10$. Otherwise, it is radio quiet. The significance of this parameter is highly debated (e.g., see Padovani 2017; Lähteenmäki et al. 2018).

this reason, an NLS1 with an elliptical host galaxy may have a high-mass black hole, and possibly a different nature.

A number of very nearby radio-quiet (or non-jetted; Padovani 2017) NLS1s are hosted by spiral galaxies (Deo et al. 2006; Mathur et al. 2012) with a strong ongoing star formation (Sani et al. 2010) and a pseudobulge due to secular evolution (Orban de Xivry et al. 2011; Mathur et al. 2012). In radio-loud (or jetted, namely harboring a relativistic jet) NLS1s, instead, the host galaxy nature is still under debate with controversial results supporting both elliptical and disk hosts (Antón et al. 2008; León Tavares et al. 2014; Kotilainen et al. 2016; D’Ammando et al. 2017, 2018; Olguín-Iglesias et al. 2017; Järvelä et al. 2018).

In this paper we present the results of a study carried out on the radio-loud NLS1s (Komossa et al. 2006) IRAS 20181-2244 ($z = 0.185$) using the *Magellan* 6.5 m Walter Baade telescope of the Las Campanas Observatory, and we will put them in the framework of the previously described scenario. In Section 2 we describe the source, in Section 3 we describe the data reduction and analysis, while in Section 4 we finally discuss the results. Throughout this work, we adopt a standard Λ CDM cosmology, with a Hubble constant of $H_0 = 70 \text{ km s}^{-1} \text{ Mpc}^{-1}$, and $\Omega_\Lambda = 0.73$ (Komatsu et al. 2011).

2. IRAS 20181-2244

Initially classified as a Seyfert 2 (Elizalde & Steiner 1994), it was reclassified as an NLS1 by Halpern & Moran (1998). Its optical B -band magnitude derived from the USNO-B catalog (Monet et al. 2003) is $m_B = 16.86$, which provides an absolute magnitude of $M_B = -22.81$. Hence, IRAS 20181-2244 could formally be classified as a narrow-line type 1 quasar (Schmidt & Green 1983). However, to avoid confusion with similar sources in the literature, in the following we will stick to the NLS1 classification. For many years it has been known as a bright X-ray source from early *ROSAT* observations (Boller et al. 1992), as many other NLS1s (Boller et al. 1996), but it was recognized as a bright radio source only later (Komossa et al. 2006) with a luminosity of $3.6 \times 10^{40} \text{ erg s}^{-1}$ at 1.4 GHz. According to Komossa et al. (2006) and Foschini et al. (2015), this object has a radio spectral index of 0.50 ± 0.07 ($F_\nu \propto \nu^{-\alpha}$) around 1.4 GHz. Therefore it lies at the divide between flat- and steep-spectrum radio-loud NLS1s, with an estimated radio loudness of ~ 45 (Chen et al. 2018). Its black hole mass estimates span between $3 \times 10^6 M_\odot$ to $3.75 \times 10^7 M_\odot$ using single epoch spectroscopy (Komossa et al. 2006) and optical magnitudes (Foschini et al. 2015), respectively. Both authors provide an Eddington ratio estimate of 0.6, due to a different calculation of the bolometric luminosity. Both mass and Eddington ratio are in the typical range for NLS1s.

One of the most interesting characteristics of IRAS 20181-2244 is its remarkably high star formation rate (SFR), up to $\sim 300 M_\odot \text{ yr}^{-1}$ (Caccianiga et al. 2015). This value is the highest among known radio-loud NLS1s, and typical for sources in the ultraluminous infrared galaxies regime (Sanders et al. 1988). Despite this surprisingly high value, the SFR is not enough to explain the totality of the radio emission. Indeed, assuming an SFR of $300 M_\odot \text{ yr}^{-1}$ and using the relation between the SFR and radio luminosity at 1.4 GHz of Condon et al. (2002), we derive an expected radio luminosity due to star formation that can explain at most $\sim 30\%$ of the observed luminosity. Therefore, the presence of the nonthermal emission of a relativistic jet is required. We note that even considering

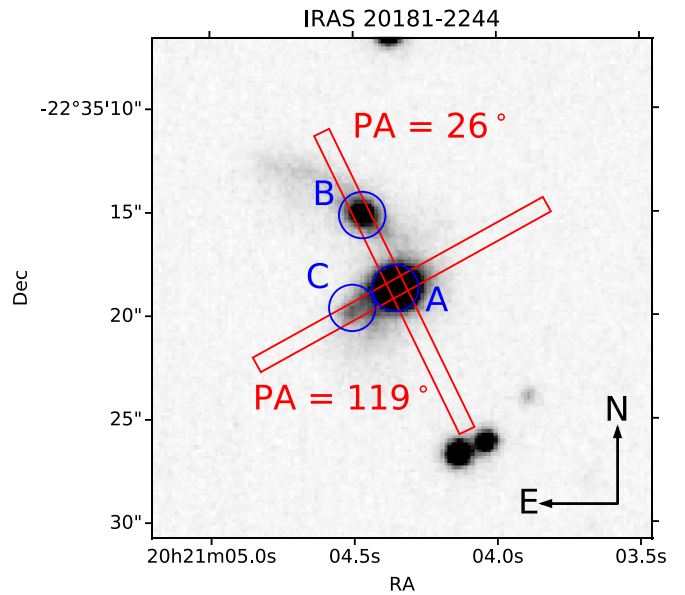


Figure 1. Finding chart of IRAS 20181-2244 (marked as A) and its putative companion sources B and C. The red boxes represent the position of the slit during the Nordic Optical Telescope observations. The two sources in the southwest are stars.

the possible amount of radio emission due to star formation, the radio-loudness parameter would be lower, but still above the formal limit of radio-loud AGN. This makes IRAS 20181-2244 a unique source worth of a detailed investigation.

3. Data Reduction and Analysis

We observed IRAS 20181-2244 on 2016 October 13 with the FourStar instrument of the Walter Baade 6.5 m telescope of the Las Campanas Observatory. We acquired images in J , H , and K_s bands, with a total exposure time of 256 s in K_s , 640 s in H , and 640 s in the J band. The seeing was $0''.67$ in the K_s band and $0''.72$ in J and H bands. The detector scale is $0''.159 \text{ px}^{-1}$, corresponding to $0.473 \text{ kpc px}^{-1}$. We performed a standard reduction using IRAF,¹⁷ with bias and flat field correction, followed by the alignment, sky subtraction, fringing removal, and a combination of the images in each filter. We later estimated the zeropoint (zp) for photometric calibration of each filter by comparing the instrumental magnitudes of some of the stars in the field, measured with point-spread function (PSF) photometry, with their 2MASS magnitudes. The resulting zps were $zp_H = 25.64 \pm 0.29$, $zp_J = 26.01 \pm 0.14$, and $zp_{K_s} = 25.12 \pm 0.18$.

The source has a rather complicated structure. In addition to the AGN and its host galaxy (component A in Figure 1), we observe a nearby galaxy at a position angle (P.A.) of 26° (component B in Figure 1). We also identify an extended emission at a P.A. of 119° , which might be a point-like source distorted by seeing, and therefore another possible galaxy (component C in Figure 1). All of the other objects surrounding the system are instead confirmed stars. To investigate the nature of the putative companions, we decided to carry out spectroscopic observations to determine their redshifts.

¹⁷ <http://iraf.noao.edu/>

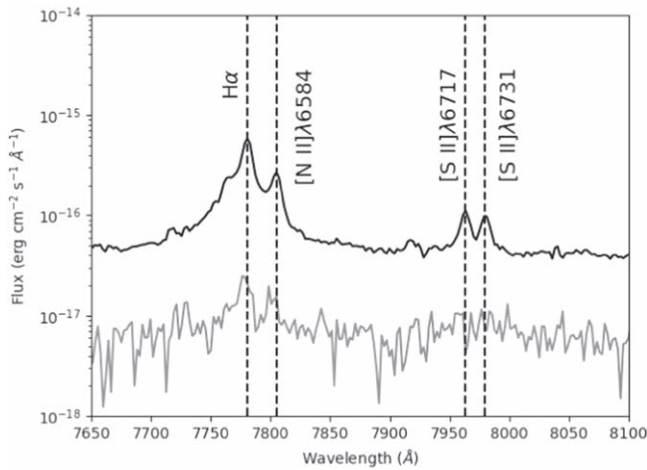


Figure 2. Spectra of IRAS 20181-2244 (black line) and its putative companion B (gray line) at P.A. = 26° in the $H\alpha$ region. The flux scale is logarithmic to enhance the lines of the companion. The dashed vertical lines mark the most prominent lines.

3.1. Spectroscopy

We observed IRAS 20181-2244 with the Nordic Optical Telescope (NOT) on 2017 August 4 and 2017 August 11. To this aim we acquired two spectra at two different P.A.s (P.A. = 26° and P.A. = 119°) to include in each observation of the nucleus of the AGN and one of the two putative companion sources. The observations were performed using the Andalucia Faint Object Spectrograph and Camera. We used a $0''.5$ slit and the grism 20, covering a spectral range from 5650 to 10150 \AA with a resolution of $R \sim 1540$. For each P.A. we acquired three spectra for a total exposure time of 1800 s at P.A. = 26° and 2700 s at P.A. = 119° . A spectrum of the standard star Feige 110 was acquired for flux calibration while a ThAr lamp and standard flat fields were acquired for wavelength calibration and flat field correction. A standard calibration procedure has been carried out using IRAF tasks.

In the NLS1 spectrum all of the most prominent Balmer lines, along with [O III] $\lambda\lambda 4959, 5007$, He I $\lambda 5876$, [O I] $\lambda 6300$, [N II] $\lambda\lambda 6548, 6584$, and [S II] $\lambda\lambda 6716, 6731$ are detected. After correcting for telluric absorption, to measure the width of the broad line we decomposed the $H\alpha$ line profile using three Gaussians. Two Gaussians are needed to represent the broad component, because its complex profile is suggestive of two different kinematic regions, as usually observed in broad-line profiles (e.g., Popović et al. 2004). A third one is instead used to represent the narrow component. We obtained $\text{FWHM}_{\text{broad}} \sim 1500 \text{ km s}^{-1}$, thus confirming the NLS1 nature of this source.

At P.A. = 26° the AGN emission lines seem to be extended up to a region where we clearly detect a faint continuum and weak emission lines ($H\alpha$ and [N II] $\lambda 6584$ are detected; see Figure 2). Both lines and continuum are located $\sim 3''.5$ away from the NLS1 nucleus, in the same position as source B in Figure 1. We tested the hypothesis that these lines originate in the AGN and are extended over source B because of the seeing. However, neither lines nor continuum were detected on the opposite side of source A, thus ruling out the seeing origin. Another possibility is that the observed lines are due to the extended narrow-line region (ENLR) of the AGN. Nevertheless, no emission lines shifted with respect to those of the putative ENLR were detected in the spectrum. Therefore, if this

Table 1
Parameters Derived from the GALFIT Fitting

R.A.	Decl.	mag.	R_e	n
PSF A (disk case)				
20:21:04.4	-22:35:18.7	13.41		
Sérsic A (disk case)				
20:21:04.4	-22:35:19.0	14.22	5.56 (1.87)	1
PSF A (elliptical case)				
20:21:04.4	-22:35:18.7	13.73		
Sérsic A (elliptical case)				
20:21:04.4	-22:35:18.7	13.71	7.44 (2.50)	4
Sérsic B (bulge)				
20:21:04.5	-22:35:15.0	16.24	0.29 (0.10)	0.51
Sérsic B (host)				
20:21:04.5	-22:35:15.0	14.82	5.81 (1.95)	1

Note. Each component is indicated in boldface. Columns: (1) R.A. (hh:mm:ss); (2) decl. (dd:mm:ss); (3) Integrated K_s magnitude; (4) effective radius in kpc (and arcsec); (5) Sérsic index.

is the case and source B emits some lines (a likely possibility given its disk nature), they are blended with those of the ENLR because of the vicinity of the two sources. The final option is simply that the observed lines originate in source B, confirming that both A and B are at the same $z = 0.185$.

In the spectrum at P.A. = 119° some emission lines from IRAS 20181-2244 are instead projected onto source C. This source, in fact, is much closer to the AGN with respect to the previous case, and the observations were performed with a seeing around $1''.5$. However, no emission or absorption lines are detected from source C itself, implying that it is either an inactive galaxy, or that it has faint emission lines at the same redshift as the NLS1, which are not detectable. In conclusion, nothing can be said about the nature of source C with our data.

3.2. Imaging

To investigate the morphology of our target we used GALFIT (Peng et al. 2002, 2010). We carried out the procedure only in the K_s band. Given the worse seeing conditions during the observations ($0''.75$ in H, J band versus $0''.67$ in K_s) and the lower quality of the H and J band due to strong fringing, we could not obtain any additional information in the other filters with respect to the K_s band. We initially reproduced the AGN with a PSF described by a Moffat function to find its exact position. The PSF profile was estimated by measuring and averaging the PSFs of 20 non-saturated stars in the field of view. As a second step we reproduced source B, fitting it with a combination of two Sérsic profiles, one for the bulge and one for the exponential disk. After obtaining a suitable result, we added a Sérsic profile to reproduce the host galaxy of the AGN. Finally, we also tried to model component C using a Sérsic profile, but we could not obtain any reliable result. The parameters derived from the fitting procedure are summarized in Table 1. Given that the nuclear PSF is dominating over the center of the galaxy

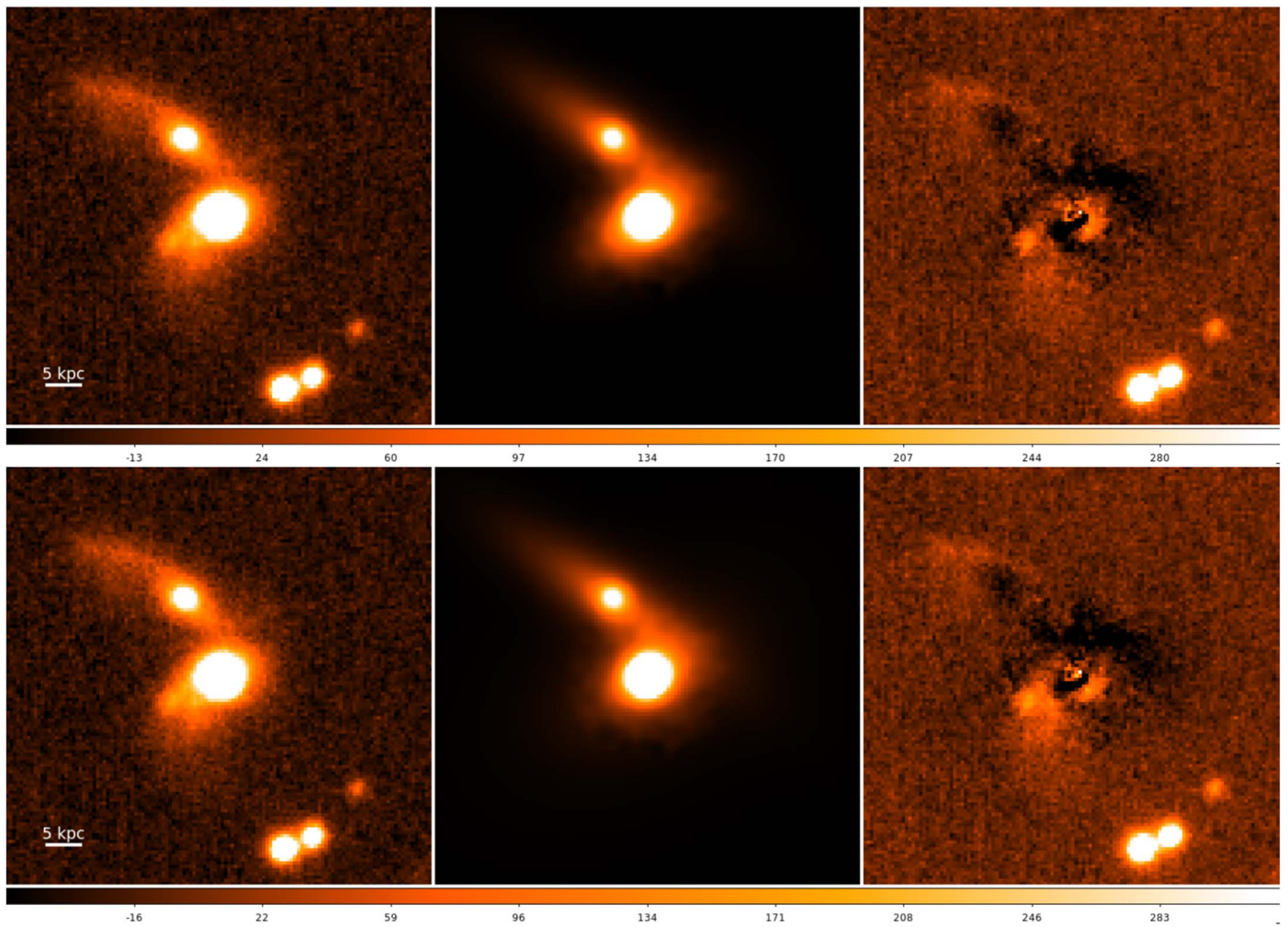


Figure 3. Left: K_s band image of IRAS 20181-2244. Middle: GALFIT model of the NLS1 and its companion. Right: residuals of the GALFIT modeling. The top row refers to the disk host model, and the bottom row to the elliptical host model. The color scale is shown below both rows. The spatial scale at the AGN redshift is indicated in both images. The orientation is that same as that in Figure 1.

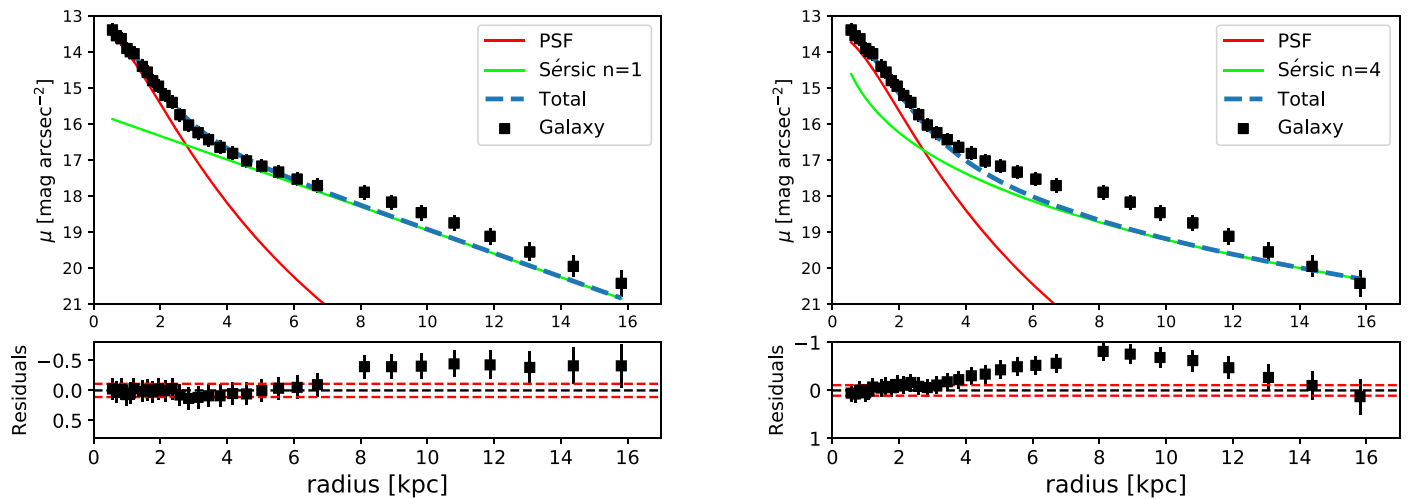


Figure 4. Brightness profile of the IRAS 20181-2244 modeling. The input parameters are those derived by GALFIT. Left panel (top): the black squares represent the isophotes of the galaxy, the red solid line represents the PSF, the green solid line represents the host galaxy model with a Sérsic index of $n = 1$ (exponential disk), and the blue dashed line indicates the total model. Bottom left panel: residuals after model subtraction; the dashed black line represents the zero level and the dashed red lines indicate the background noise level. Right panel: as in the left panel, but the host galaxy model has a Sérsic index of $n = 4$.

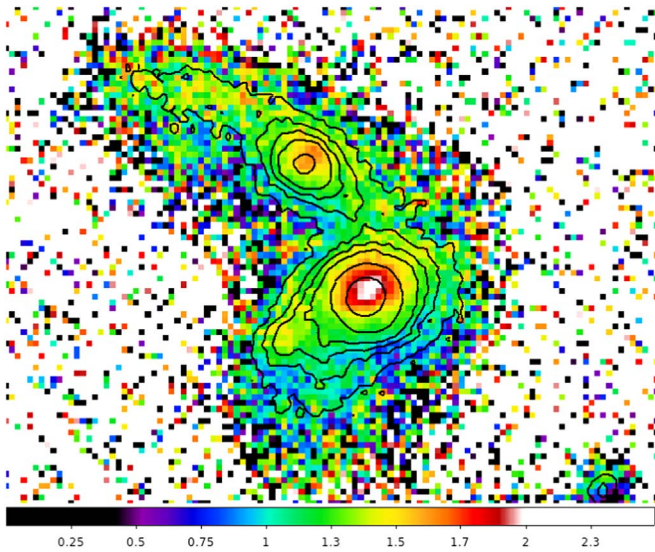


Figure 5. $J-K_s$ color of IRAS 20181-2244. The color scale is reported at the bottom of the image. The contour levels represent 10, 20, 30, 45, 100, and 400 times the rms calculated on the K_s band image.

because of the seeing, we decided to avoid trying to reproduce both the bulge and the host, but to focus only on the latter.

With no constraint, its Sérsic index converged to 0.29, suggesting a late-type nature for the host. To derive the physical parameters of the host properly, we re-fitted it with an exponential disk (Sérsic index $n = 1$), obtaining a reduced- χ^2 (χ^2_ν) = 1.567. The original K_s image, the model produced by GALFIT, and the residual image are shown in the top row of Figure 3. For further confirmation of the GALFIT results, we also extracted the brightness profile of the AGN host galaxy using the IRAF task `ellipse`, while masking companion B. The result is shown in the left panel of Figure 4. The parameters used to reproduce the profile are those already derived by GALFIT.

We also tried to reproduce the host galaxy profile with a Sérsic with index of $n = 4$, which represents the brightness profile of an elliptical galaxy, along with the nuclear PSF. This attempt led to $\chi^2_\nu = 1.739$, higher than that obtained for the disk model. The GALFIT modeling is shown in the bottom row of Figure 3, while the brightness profile is displayed in the right panel of Figure 4.

We also estimated the $J-K_s$ color of the galaxy. Given that the shape of the near-infrared spectrum is not known, we did not K -correct the different bands. The resulting map is shown in Figure 5.

4. Discussion

Because of the seeing, the nuclear region is dominated by the PSF of the AGN. This prevented any modeling of a potential bulge component. As shown in Figure 4, in fact, no additional component is needed besides the host and the PSF to reproduce the brightness profile of the inner regions of this galaxy.

Regarding the host, as shown in Table 1 and Figures 3 and 4, the PSF + exponential disk model can reproduce quite well the outer regions of the galaxy up to 8 kpc, but it fails at larger radii, where a significant deviation is observed. However, this flux excess may be due to the presence of component C, which was not modeled and lies at ~ 8 kpc ($\sim 2''6$) away from the nucleus (assuming it is at the same redshift as the AGN).

The elliptical host + PSF model instead seems to reproduce the data only up to 4 kpc from the nucleus. At larger distances, the data lie systematically above the model predictions, and only at very large radii (>13 kpc) the model seems to be again in agreement with the observations. Another weakness of this model is that the brightness profile of the elliptical host is significantly higher in the nuclear region with respect to the disk, and its peak magnitude is almost comparable to that of the AGN. If true, in the optical spectrum we would expect to observe at least some absorption lines and the 4000 Å break that, instead, are not observed. Therefore, despite some data limitations, we are inclined to believe that the disk model is a better representation of the host galaxy.

As mentioned above, the significant deviation from the exponential profile at large radii may be associated with component C. Its nature is not certain yet. The optical spectrum of this region, given its relatively small distance from the nucleus, was dominated by the AGN, and therefore it was not possible to fully determine whether it is a bright star-forming region, a small galaxy interacting with the AGN host, or a tidal tail produced by the interaction between components A and B. Conversely, source B is a late-type galaxy, well reproduced by a Sérsic profile for the bulge with the addition of an exponential profile for the disk. This object also shows a luminosity excess in the residuals, which is suggestive of a tidal tail produced by its interaction with the AGN host.

The color index $J-K_s$ provides some additional information. In the NLS1 nucleus its value is ~ 2.1 . This result is not far from typical colors observed in other AGN (Fischer et al. 2006; Masci et al. 2010), even if this one seems to be slightly redder when compared to other quasars (Leipski et al. 2007). A small fraction of this very red color (around ~ 0.2) could be attributed to the lack of K -correction in our data, but despite this the nucleus is definitely very red. The reason for this could be a combination of dust absorption and host dilution. The nucleus of the companion galaxy is also fairly red (~ 1.6), showing that dust might be very abundant in both of these interacting galaxies. The colors could also be an indication that there is a significant ongoing star formation activity in the reddest parts of the system. The star formation indeed is responsible for a significant Pa α emission which, because of the redshift, falls in the K_s band lowering its magnitude. In particular, the inner 3 kpc of the nucleus, source C, and the tidal tail of source B might all possibly contribute to the extreme SFR observed in this galaxy by Caccianiga et al. (2015).

The ongoing interaction that we observe might play a key role in the relativistic jet production. In high-mass jetted AGN, for example, merging and interaction are frequently observed (Chiaberge et al. 2015). If jetted AGN are associated with rapidly spinning black holes, merging can help to spin up the black hole via several accretion episodes, thus triggering the relativistic jet launching. If this is true, among NLS1s, non-jetted sources might have a lower spin with respect to jetted NLS1s (e.g., Chiaberge et al. 2017, and references therein), since they tend not to show merging episodes (Krongold et al. 2001; Xu et al. 2012). This lack of frequent interactions found among non-jetted NLS1s might be a consequence of their large-scale environment, which is different with respect to that of jetted NLS1s (Järvälä et al. 2017a, 2017b). Galaxies that reside in a dense environment, on average, have a higher probability to interact with other sources than galaxies located in voids. Even if the relative velocity between galaxies and the





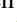
position of each galaxy within its environment also play a role in the process, we can conclude that a dense environment may usually produce a higher fraction of jetted sources.

In conclusion, if the disk host hypothesis for IRAS 20181-2244 is correct, this NLS1 (we remark that formally this object is classifiable as a quasar) is hosted by a galaxy with a scale radius of 3.3 kpc, slightly larger than that of the Milky Way in the same band (Porcel et al. 1998). This source, then, may belong to the class of disk-hosted jetted NLS1s, as some other similar objects found in the literature (Antón et al. 2008; Kotilainen et al. 2016; Olguín-Iglesias et al. 2017; Järvelä et al. 2018). The presence of jetted NLS1s hosted also in elliptical galaxies (D’Ammando et al. 2017, 2018) suggests that both classes of jetted NLS1s exist. In a similar fashion, evidence for two different classes of NLS1s has already been discussed in the literature, based for instance on the spread of X-ray slopes, on the range of Eddington ratios, and the strength (or weakness) of Fe II emission (e.g., Xu et al. 1999; Sulentic et al. 2000; Williams et al. 2004; Mathur & Grupe 2005a, 2005b, and references therein). We speculate that, while disk-hosted sources are characterized by young age and fast evolution (Foschini et al. 2015; Berton et al. 2016, 2017; Komossa 2018), the others may be instead low-inclination, and possibly not young, sources that mimic the behavior of genuine NLS1s. Further morphological studies on jetted and non-jetted NLS1s are needed to confirm or disprove this scenario, and to shed more light on the formation of relativistic jets in this intriguing class of AGN.

This paper is based on observations made with the Nordic Optical Telescope, operated by the Nordic Optical Telescope Scientific Association at the Observatorio del Roque de los Muchachos, La Palma, Spain, of the Instituto de Astrofísica de Canarias. J.K. acknowledges financial support from the Academy of Finland, grant 311438. S.A. acknowledges support from CIDMA strategic project (UID/MAT/04106/2013), ENGAGE SKA (POCI-01-0145-FEDER-022217), funded by COMPETE 2020 and FCT, Portugal. We are grateful to M. Baratella, I. Pagotto, and E. Sissa for helpful suggestions. This research has made use of the NASA/IP.A.C Extragalactic Database (NED) which is operated by the Jet Propulsion Laboratory, California Institute of Technology, under contract with the National Aeronautics and Space Administration. The National Radio Astronomy Observatory is a facility of the National Science Foundation operated under cooperative agreement by Associated Universities, Inc. Funding for the Sloan Digital Sky Survey (SDSS) has been provided by the Alfred P. Sloan Foundation and the U.S. Department of Energy Office of Science. The SDSS website is <http://www.sdss.org>. SDSS-III is managed by the Astrophysical Research Consortium for the Participating Institutions of the SDSS-III Collaboration including the University of Arizona, the Brazilian Participation Group, Brookhaven National Laboratory, Carnegie Mellon University, University of Florida, the French Participation Group, the German Participation Group, Harvard University, the Instituto de Astrofísica de Canarias, the Michigan State/Notre Dame/JINA Participation Group, Johns Hopkins University, Lawrence Berkeley National Laboratory, Max Planck Institute for Astrophysics, Max Planck Institute for Extraterrestrial Physics, New Mexico State University, University of Portsmouth, Princeton University, the Spanish Participation Group, University of Tokyo, University of Utah, Vanderbilt University, University of Virginia, University of

Washington, and Yale University. This research has made use of Aladin sky atlas developed at CDS, Strasbourg Observatory, France.

ORCID iDs

M. Berton  <https://orcid.org/0000-0002-1058-9109>
 E. Congiu  <https://orcid.org/0000-0002-8549-4083>
 S. Ciroi  <https://orcid.org/0000-0001-9539-3940>
 S. Komossa  <https://orcid.org/0000-0002-9214-4428>
 F. Di Mille  <https://orcid.org/0000-0003-0483-5083>
 S. Antón  <https://orcid.org/0000-0002-0658-644X>
 A. Caccianiga  <https://orcid.org/0000-0002-2339-8264>
 J. Kotilainen  <https://orcid.org/0000-0003-0133-7644>
 G. La Mura  <https://orcid.org/0000-0001-8553-499X>
 P. Rafanelli  <https://orcid.org/0000-0002-6717-1686>

References

- Abdo, A. A., Ackermann, M., Ajello, M., et al. 2009a, *ApJ*, 699, 976
 Abdo, A. A., Ackermann, M., Ajello, M., et al. 2009b, *ApJL*, 707, L142
 Antón, S., Browne, I. W. A., & Marchã, M. J. 2008, *A&A*, 490, 583
 Berton, M., Caccianiga, A., Foschini, L., et al. 2016, *A&A*, 591, A98
 Berton, M., Congiu, E., Järvelä, E., et al. 2018, *A&A*, 614, A87
 Berton, M., Foschini, L., Caccianiga, A., et al. 2017, *FrASS*, 4, 8
 Boller, T., Brandt, W. N., & Fink, H. 1996, *A&A*, 305, 53
 Boller, T., Meurs, E. J. A., Brinkmann, W., et al. 1992, *A&A*, 261, 57
 Boroson, T. A., & Green, R. F. 1992, *ApJS*, 80, 109
 Caccianiga, A., Antón, S., Ballo, L., et al. 2015, *MNRAS*, 451, 1795
 Chen, S., Berton, M., La Mura, G., et al. 2018, *A&A*, 615, A167
 Chiaberge, M., Ely, J. C., Meyer, E. T., et al. 2017, *A&A*, 600, A57
 Chiaberge, M., Gilli, R., Lotz, J. M., & Norman, C. 2015, *ApJ*, 806, 147
 Chiaberge, M., & Marconi, A. 2011, *MNRAS*, 416, 917
 Condon, J. J., Cotton, W. D., & Broderick, J. J. 2002, *AJ*, 124, 675
 D’Ammando, F., Acosta-Pulido, J. A., Capetti, A., et al. 2017, *MNRAS*, 469, L11
 D’Ammando, F., Acosta-Pulido, J. A., Capetti, A., et al. 2018, *MNRAS*, 478, L66
 Decarli, R., Dotti, M., Fontana, M., & Haardt, F. 2008, *MNRAS*, 386, L15
 Deo, R. P., Crenshaw, D. M., & Kraemer, S. B. 2006, *AJ*, 132, 321
 Elizalde, F., & Steiner, J. E. 1994, *MNRAS*, 268, L47
 Ferrarese, L., & Merritt, D. 2000, *ApJL*, 539, L9
 Fischer, S., Iserlohe, C., Zuther, J., et al. 2006, *A&A*, 452, 827
 Foschini, L. 2011, *RAA*, 11, 1266
 Foschini, L., Berton, M., Caccianiga, A., et al. 2015, *A&A*, 575, A13
 Goodrich, R. W. 1989, *ApJ*, 342, 224
 Halpern, J. P., & Moran, E. C. 1998, *ApJ*, 494, 194
 Heinz, S., & Sunyaev, R. A. 2003, *MNRAS*, 343, L59
 Järvelä, E., Lähteenmäki, A., & Berton, M. 2018, *A&A*, 619, A69
 Järvelä, E., Lähteenmäki, A., & Lietzen, H. 2017a, *FrASS*, 4, 54
 Järvelä, E., Lähteenmäki, A., Lietzen, H., et al. 2017b, *A&A*, 606, A9
 Kawakatu, N., Imanishi, M., & Nagao, T. 2007, *ApJ*, 661, 660
 Kellermann, K. I., Sramek, R., Schmidt, M., Shaffer, D. B., & Green, R. 1989, *AJ*, 98, 1195
 Komatsu, E., Smith, K. M., Dunkley, J., et al. 2011, *ApJS*, 192, 18
 Komossa, S. 2018, Revisiting narrow-line Seyfert 1 galaxies and their place in the Universe (Trieste: PoS), 15
 Komossa, S., Voges, W., Xu, D., et al. 2006, *AJ*, 132, 531
 Kormendy, J., & Ho, L. C. 2013, *ARA&A*, 51, 511
 Kotilainen, J. K., León-Tavares, J., Olguín-Iglesias, A., et al. 2016, *ApJ*, 832, 157
 Krongold, Y., Dultzin-Hacyan, D., & Marziani, P. 2001, *AJ*, 121, 702
 Lähteenmäki, A., Järvelä, E., Ramakrishnan, V., et al. 2018, *A&A*, 614, L1
 Laor, A. 2000, *ApJL*, 543, L111
 Leipski, C., Haas, M., Siebenmorgen, R., et al. 2007, *A&A*, 473, 121
 León Tavares, J., Kotilainen, J., Chavushyan, V., et al. 2014, *ApJ*, 795, 58
 Mao, M. Y., Owen, F., Duffin, R., et al. 2015, *MNRAS*, 446, 4176
 Masci, F. J., Cutri, R. M., Francis, P. J., et al. 2010, *PASA*, 27, 302
 Mathur, S. 2000, *MNRAS*, 314, L17
 Mathur, S., Fields, D., Peterson, B. M., & Grupe, D. 2012, *ApJ*, 754, 146
 Mathur, S., & Grupe, D. 2005a, *A&A*, 432, 463
 Mathur, S., & Grupe, D. 2005b, *ApJ*, 633, 688
 Mathur, S., Kuraskiewicz, J., & Czerny, B. 2001, *NewA*, 6, 321

- Monet, D. G., Levine, S. E., Canzian, B., et al. 2003, *AJ*, **125**, 984
- Olguín-Iglesias, A., Kotilainen, J. K., León Tavares, J., Chavushyan, V., & Añorve, C. 2017, *MNRAS*, **467**, 3712
- Orban de Xivry, G., Davies, R., Schartmann, M., et al. 2011, *MNRAS*, **417**, 2721
- Osterbrock, D. E., & Pogge, R. W. 1987, *ApJ*, **323**, 108
- Padovani, P. 2017, *NatAs*, **1**, 0194
- Peng, C. Y., Ho, L. C., Impey, C. D., & Rix, H.-W. 2002, *AJ*, **124**, 266
- Peng, C. Y., Ho, L. C., Impey, C. D., & Rix, H.-W. 2010, *AJ*, **139**, 2097
- Peterson, B. M. 2011, in *Narrow-Line Seyfert 1 Galaxies and their Place in the Universe*, ed. L. Foschini et al. (Trieste: PoS), 32
- Popović, L. Č., Mediavilla, E., Bon, E., & Ilić, D. 2004, *A&A*, **423**, 909
- Porcel, C., Garzon, F., Jimenez-Vicente, J., & Battaner, E. 1998, *A&A*, **330**, 136
- Salucci, P., Ratnam, C., Monaco, P., & Danese, L. 2000, *MNRAS*, **317**, 488
- Sanders, D. B., Soifer, B. T., Elias, J. H., et al. 1988, *ApJ*, **325**, 74
- Sani, E., Lutz, D., Risaliti, G., et al. 2010, *MNRAS*, **403**, 1246
- Schmidt, M., & Green, R. F. 1983, *ApJ*, **269**, 352
- Shen, Y., & Ho, L. C. 2014, *Natur*, **513**, 210
- Sulentic, J. W., Zwitter, T., Marziani, P., & Dultzin-Hacyan, D. 2000, *ApJL*, **536**, L5
- Wang, J.-M., & Zhang, E.-P. 2007, *ApJ*, **660**, 1072
- Williams, R. J., Mathur, S., & Pogge, R. W. 2004, *ApJ*, **610**, 737
- Xu, D., Komossa, S., Zhou, H., et al. 2012, *AJ*, **143**, 83
- Xu, D. W., Wei, J. Y., & Hu, J. Y. 1999, *ApJ*, **517**, 622